

Creep Properties Identification of PBX Using Digital Image Correlation

Baoqiao Guo^a; Huimin Xie^{*a}; Pengwan Chen^b; Qingming Zhang^b

^aAML, Department of Engineering Mechanics, Tsinghua University, Beijing, China; ^bState Key Laboratory of Explosion Science and Technology, Beijing Institute of Technology, Beijing, China

ABSTRACT

The creep behavior of the polymer bonded explosive (PBX) substitute material is investigated by using the digital image correlation (DIC) method. At first step the 3-points bending test is applied to achieve the tested PBX substitute material's elastic parameters, which are identified by the calculated heterogeneous strain fields and the so-called virtual fields method (VFM). In the second step, the creep property of PBX material is studied by the Brazilian disc compression test. The stress fields could then be reconstructed with the identified elastic parameters and the strain fields at the first step of loading. The time hardening coefficients which present the creep behavior could be extracted by the time-depending strain rate curves of the points on the surface.

Keywords: Polymer Bonded Explosive (PBX), digital image correlation (DIC), elastic, creep, virtual fields method (VFM), 3- points bending.

1. INTRODUCTION

The polymer bonded explosives (PBX) materials are a polymer matrix composites filled with high percent explosive granule. PBXs have a large ranging application, normally used such as rocket propellants and the explosive materials. Because of their dangerous specialty during the manufacture, transport and storage, it's of great importance to determine their mechanical properties in various conditions.

Many investigations have been performed in the literature to evaluate the security and reliability of PBX by the study on the mechanical properties. The PBX of low percent polymer matrix is a typical viscoelastic material, damage and creep deformation is inevitable during storage and transport, especially at high temperatures. By using compression tests on standard cylinder specimens, Li et al. have shown the strong temperature dependence of Modulus and failure strength of PBX¹. Compressive creep results in high strain at different temperatures also showed the creep behavior has great influence to PBX's mechanical properties. The important creep parameters could be achieved. Using Brazilian disc tests by various loadings, Chen et al. studied PBX material failure evolution in a microstructure scale². Different style damages were observed and analyzed. They also studied the creep behavior by using cylinder specimen.

As an alternative, Xie et al. studied PBX creep behavior on a compressive disc specimen by using a high-resolution full-field method: moiré interferometry³. The heterogeneous stress/strain fields resulted in the difficulty of measurement, but creep curves on different points of the observed surface could be achieved just by one test. Liu et al. studied the failure and creep behavior of PBX by combined thermal and mechanical loads, in which DIC method was applied to investigate the strain fields of PBX specimen⁴. The author studied the relation between the failure and the creep. However, only creep curves were shown in above, the intrinsic creep parameters were not investigated.

The objective of this work is to study the PBX like material creep properties by using the DIC method. The time hardening creep model is applied. The creep parameters of this kind model would be achieved. Simple tensile/compression test on standard specimen is a traditional way to study mechanical property. Homogenous strain/stress fields make it easy to get the creep curve, whereas the test should be repeated several times with different loadings to achieve the material's creep parameters just as the method in previous study¹.

* xiehm@mail.tsinghua.edu.cn ; Phone: +86-10-62792286

As an alternative, 3-points bending test, which achieve heterogeneous strain/stress fields, is applied in this study. Full displacement fields of observed surface are measured by DIC. At first step the elastic properties are identified by the calculated strain fields and the VFM. The stress field would then be reconstructed. Secondly, time-depending strain fields of many steps would be calculated. The time-depending deformed images of many steps would be recorded. The full displacement/deformation fields are achieved by DIC method. The time hardening parameters which present the creep behavior could be extracted by the time-depending strain rate curves of all points on the surface. In this paper the tests were performed in the room temperature. The study on creep properties would be applied in different temperatures.

2. ELASTIC TEST

2.1 Experimental set-up

The PBX substitute material in this study is constituted by small glass bead (80% in weight) and epoxy polymer (20%) in weight. At first the two constituents of non- solidified epoxy are mixed by a centrifuge of 1500 r/min more than 10 minutes. The (rectangular and cylinder) specimens are prepared with the mixture of glass bead and epoxy in suitable moulds in ambient environment.

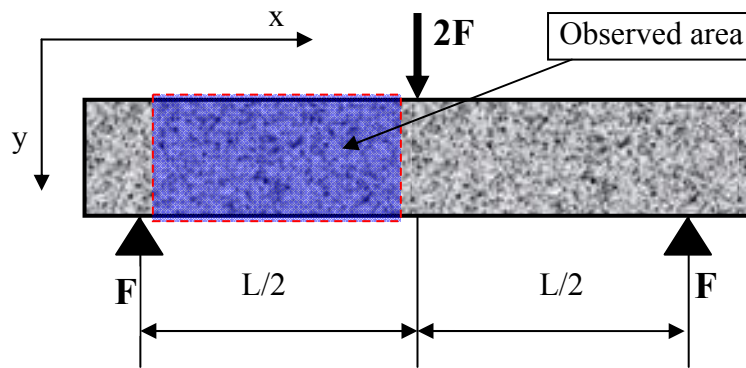


Figure 1. Schematic of the 3-points bending on rectangular specimen

The first phase of work concerns the identification of the elastic parameters. The rectangular specimen (dimensions: $120 \times 20 \times 10 \text{ mm}^3$) was used in the 3-points bending test (see Figure 1). The specimen is installed on a tension/compression machine. The distance between two supporting points is 110mm. A set of load is applied by the machine. The images of specimen are taken by using a Daheng CMOS camera (8-bit, 1.3M pixels) with a 12.5-75mm AVENIR lens. The surface of specimen was colored with white painter background and with black random speckle which made a good random speckle surface for the full kinematical fields calculation by DIC method.

2.2 Image processing for full fields measurement

Recently, the digital image correlation (DIC) method is now widely applied in experimental mechanics as a practical and effective tool for full field measurement⁵. This method is easy to manipulate and can provide satisfactory resolution of displacement/strain fields^{6,7}.

The correlation windows used here are 31×31 pixels with shifting size 4 pixels. The displacement field is a matrix of 127×255 points. The physical length of the pixel is 31 microns. The raw non-filtered displacement fields are shown in Figure 2 (where loading is 632.2N). The displacement fields are smoothed and the strain fields are achieved basing on 3-nodes triangular finite elements pieces⁸ (bilinear triangular element type). The nodal displacements are determined by adjusting the least mean squares. The strain fields are then obtained using the form function projected on the same network.

The strain fields associated achieved from a meshing size of 15 points are shown in Figure 3. We can find that the strain fields strongly depend on the triangular mesh pieces. The bilinear 3-nodes triangular element type is continuous of type C^0 , its derivation is not continuous. Whereas the strain fields achieved by this way are not nice to see, they are quite stable from the noise of measured displacement fields. The other strongpoint is that the virtual works are the sum of products of real and virtual strain fields of all points; the local diversity has little influence for the parameters identification.

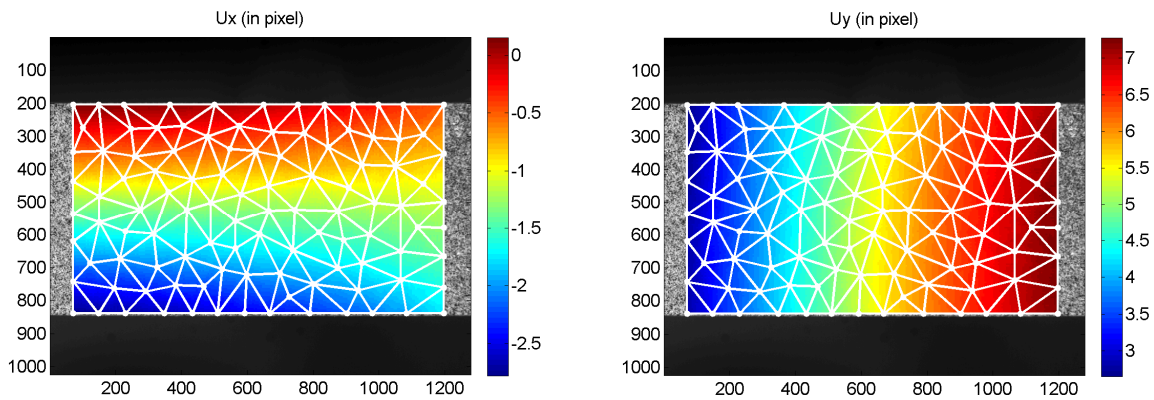


Figure 2. Measured displacement fields (non-smoothed) with triangular meshes (meshing size: 15 points) on non-deformed image

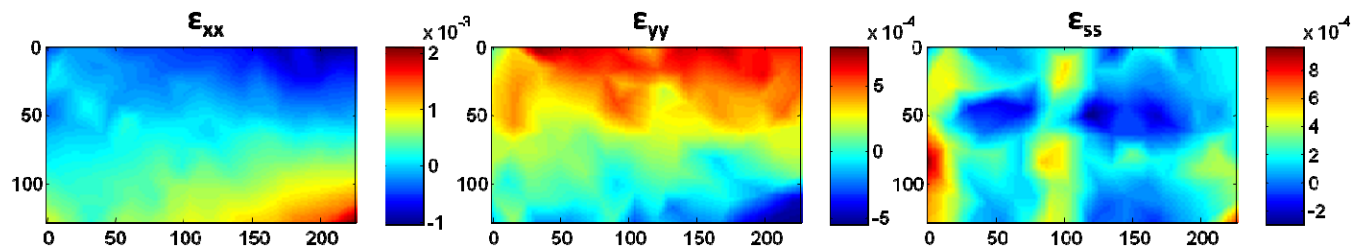


Figure 3. Reconstructed strain fields by triangular finite elements method (same mesh as in Figure 2)

2.3 Identification by the virtual fields method (VFM)

The identification of elastic parameters is effectuated by the VFM. All the constitutive parameters could be directly identified from the measured fields and the VFM, which has been developed and applied for direct material properties characterization in recent twenty years⁹. By the VFM and full-field measurement, the elasto-plastic behavior of metal is studied, as well as the stress fields are reconstructed¹⁰.

The choice of virtual fields has a great important influence on the quality of parameters' identification. Here, the optimal piecewise virtual fields defined on the same triangular meshes as the real smoothed fields (see Figure 2) can achieve the optimal solution. This point is very important with the measured noisy fields during the identification^{11,12}.

Table 1. Identified elastic parameters (Young's Modulus and Poisson's ratio) using different meshing sizes

Meshing size	E (GPa)	ν
7	14.2	0.381
10	13.8	0.384
15	13.1	0.373
20	11.2	0.402
Mean	13.1	0.351
Coef. Var.	10%	3.2%

This procedure is implemented in free software CAMFIT (www.camfit.fr), in which the image processing and the parameters identification routine are packaged. By using this software, previous study on soft foam was performed by a cantilever beam bending test¹³, which is quite similar to the 3-points test in this study. The only critical parameter in this software is the meshing size. The identified results are shown in Table 1 by using different meshing sizes.

The results of identification are shown in Table 1. We can see that the results depend very little on the mesh size, indicating a stable identification and therefore satisfactory. We see that the variation coefficient is higher for the Poisson's ratio. The results by meshing size 10 are considered as the material elastic parameters. Actually, the strain level is quite weak (see Figure 3), so the measuring noise has a quite important influence for the identification. When the loading is more 700N, the specimen is broken in two parts in the middle. The test material is a typical fragile, the maximum strain is on the loading point, the mean strain level of the studied zone is relatively very poor. So the noisy effect could not be reduced by this way. Therefore, the study on creep behavior is performed by disc specimen compression test. The elastic parameters identified by this step would be employed for the creep characterization in the next step.

3. CREEP TEST

3.1 Time-hardening creep model

Previous creep studies of PBX materials presented in Introduction, most works tried to investigate the influence of creep to the mechanical properties of PBX, whereas the instinct parameters relative to creep behavior are investigated here. The time-hardening creep model^{14,15} is used:

$$\dot{\epsilon}_{cr} = C_1 \sigma^{C_2} t^{C_3} e^{-C_4/T} \quad (1)$$

Where

ϵ_{cr} : equivalent creep strain

$\dot{\epsilon}_{cr}$: equivalent creep strain rate

σ : equivalent stress (von mises)

T : temperature (absolute)

C_1, C_2, C_3, C_4 : creep parameters of the time-hardening creep model

The finished tests are performed only in room temperature, so if we make $C_{14} = C_1 e^{-C_4/T}$, who will get

$$\dot{\epsilon}_{cr} = C_{14} \sigma^{C_2} t^{C_3} \quad (2)$$

Thus there are only 3 parameters to be investigated: C_{14}, C_2, C_3 , where parameter C_{14} are the combination of two parameters by ignoring the temperature. To achieve these parameters, we should get the time-depending creep strain of different stress states.

During the phenomenon of creep, the deformation increases with the time. In the elastic limit, the deformation has two parts:

$$\epsilon(t) = \epsilon_{el} + \epsilon_{cr}(t) \quad (3)$$

The elastic one ϵ_{el} and the creep one ϵ_{cr} . The former is independent of time, while the latter increases with time. So the creep stain rate is just that of total strain:

$$\dot{\epsilon}_{cr}(t) = \dot{\epsilon}(t) \quad (4)$$

The idea is to perform a heterogeneous stress/strain experimental test, the full strain fields would be taken by DIC, and the stress of all points would be calculated by elastic law and the measured strain fields.

3.2 Experimental test and image treatment

Due to the weak strain fields of the 3-points bending test (in elastic test part) on PBX substitute material, we could not get satisfactory result. So we tried the compression test on disc specimen, the specimen could not reach crack under quite great loading. A simple experimental set-up similar to previous study is used in this study.

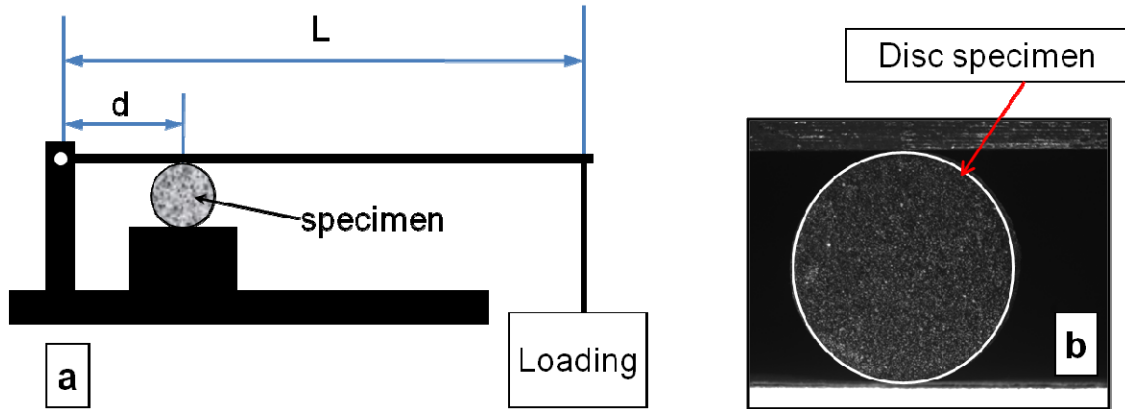


Figure 4. Disc compression creep test. (a) Schematic of the experimental set-up; (b) The raw image of the observed surface

In Figure 4(a), the loading at the end of right side is 72 Newton , where $d = 147\text{mm}$, $L = 470\text{m}$. By this way the actual charge on the disc specimen is amplified. The specimen is of dimensions $\Phi 20 \times 10\text{mm}$. The surface is treated by the same way as in Section 2, and the same camera is used to record the images. The creep test is kept during 1000 seconds, an images is taken per every 20 seconds. By DIC method, the displacement fields could be achieved in every step. The initial displacement fields (where $t = 0\text{s}$) are shown in Figure 5.

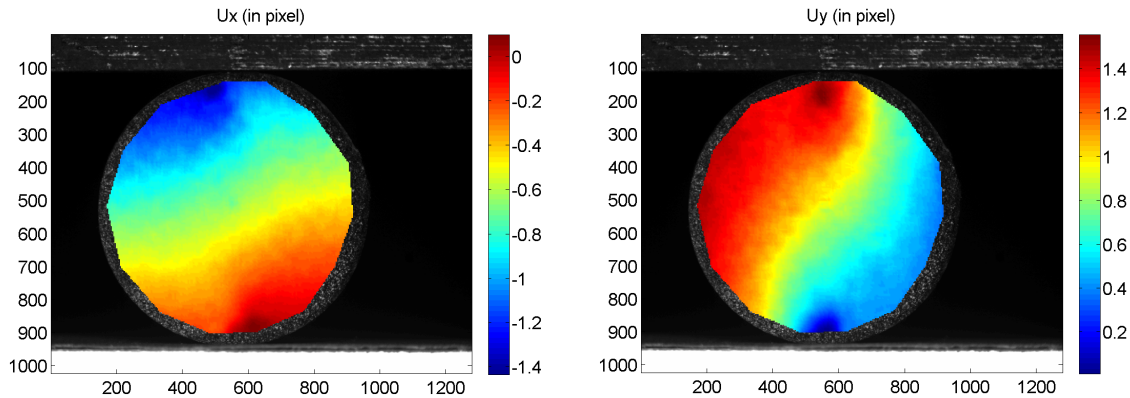


Figure 5. Measured displacement fields (non-smoothed) at the beginning of test

The correlation windows used here are 31×31 pixels with shifting size 2 pixels to calculate the displacement maps, while a 21×21 differential windows based on least-square fitting is used to calculate the strains fields. The initial elastic strain fields shown in Figure 6 is respective the displacement fields in Figure 5. We can find that maxi strains appear near the up and bottom contact zones.

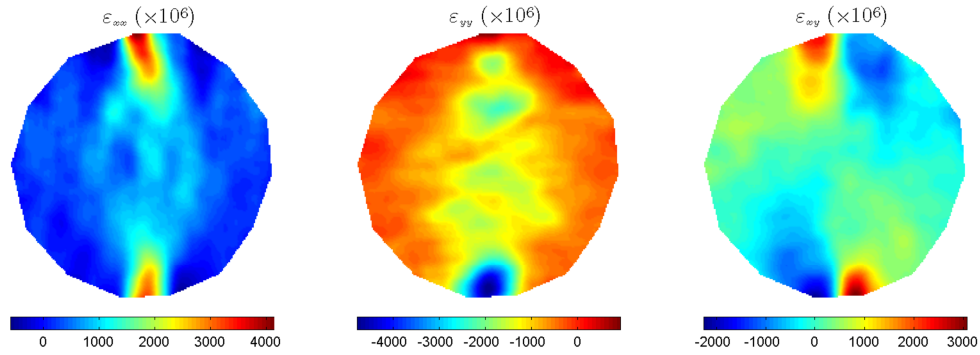


Figure 6. Elastic strain fields (at the beginning of test)

3.3 Creep parameters investigation

From Equation (2), we should analyze the stress/ strain on at least two points to get the creep parameters. Figure 7(a) shows the histogram of elastic strain ε_{xx} , and in Figure 7(b), the creep curves of ε_{xx} on some representative points in all deformation range.

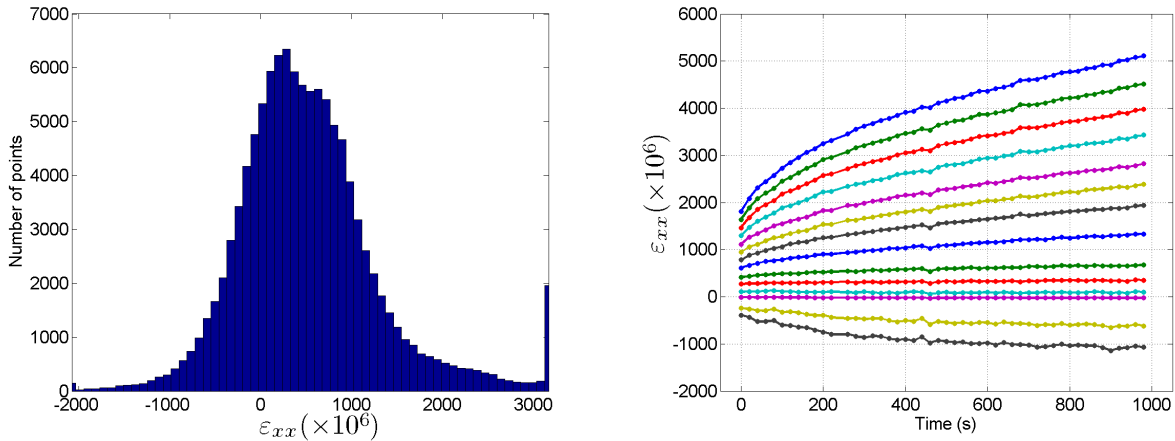


Figure 7. Tensile strain along X direction. (a) Histogram of elastic strain; (b) Creep curves of some representatives points

Actually, if the strain rate of $\dot{\varepsilon}_{xx}(t)$ is directly from the derivation of $\varepsilon_{xx}(t)$ (as shown in Figure 7(b)), $\dot{\varepsilon}_{xx}(t)$ would be much influenced by the measured noisy data. So we use the time-depending strain curves would be fitted by polynomial. Only the 6 first curves of high strain level are filtered by polynomial fitting. The same treatment applied to the other deformation components: $\varepsilon_{yy}(t)$ and $\varepsilon_{xy}(t)$. The order 4 is used to fit these curves.

$$\dot{\varepsilon}_{cr} = \sqrt{\frac{2}{3} \left[\left(\dot{\varepsilon}_{xx} \right)^2 + \left(\dot{\varepsilon}_{yy} \right)^2 + \left(\dot{\varepsilon}_{zz} \right)^2 + 2 \left(\dot{\varepsilon}_{xy} \right)^2 \right]} \quad (5)$$

By Equation (5), the equivalent creep strain rate could be achieved, where the $\dot{\varepsilon}_{zz}(t)$ is ignored. The creep strain rate of component $\dot{\varepsilon}_{xx}(t)$ is shown in Figure 8(a), corresponding to the first 6 curves in Figure 7(b). The equivalent creep strain

rate are shown in Figure 8(b). The other two components ($\dot{\epsilon}_{yy}(t)$ and $\dot{\epsilon}_{xy}(t)$) are not shown. So the part on left side of Equation (2) is achieved.

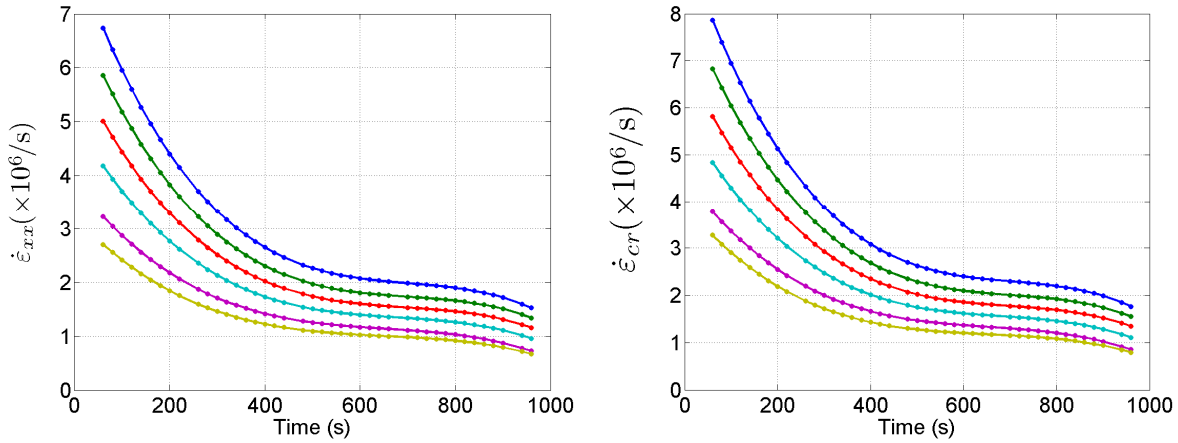


Figure 8. Creep strain rate curves (a) along X direction; (b) Equivalent creep strain rate

By Hook's law, the stress could be found by the equation below:

$$\begin{Bmatrix} \sigma_x \\ \sigma_y \\ \sigma_s \end{Bmatrix} = \begin{bmatrix} Q_{xx} & Q_{xy} & 0 \\ Q_{xy} & Q_{xx} & 0 \\ 0 & 0 & (Q_{xx} - Q_{xy})/2 \end{bmatrix} \begin{Bmatrix} \epsilon_x \\ \epsilon_y \\ \epsilon_s \end{Bmatrix}, \text{ with } Q_{xx} = \frac{E}{1-\nu^2}, \quad Q_{xy} = \frac{\nu E}{1-\nu^2} \quad (6)$$

where the stiffness parameters have been identified in Section 2, and elastic strain are measured. The von mises stress is also expressed as :

$$\sigma = \sigma_{vm} = \sqrt{\frac{(\sigma_{xx} - \sigma_{yy})^2 + (\sigma_{xx} - \sigma_{zz})^2 + (\sigma_{zz} - \sigma_{yy})^2 + 6(\sigma_{xy}^2 + \sigma_{yz}^2 + \sigma_{zx}^2)}{2}} \quad (7)$$

In case of stress plan: $\sigma_{xy} = \sigma_{yz} = \sigma_{zz} = 0$, so we will have the equivalent stress as

$$\sigma = \sqrt{\sigma_{xx}^2 + \sigma_{yy}^2 - \sigma_{xx}\sigma_{yy} + 3\sigma_{ss}^2} \quad (8)$$

Where the stress components are calculated from Equation (6). The equivalent stress are shown below.

Table 2. Equivalent stress corresponding to the points of the curves in Figure 8

Point number	1	2	3	4	5	6
σ (MPa)	43.0	39.4	36.5	33.4	29.1	25.7

From all the above experimental stress/strain data, it's quite complex to directly get the creep parameters from Equation (2). The logarithm of Equation (2) would make it is much easier, thus we can get

$$\ln\left(\dot{\epsilon}_{cr}(\sigma, t)\right) = \ln(C_{14}) + C_2 \ln(\sigma) + C_3 \ln(t) \quad (9)$$

The three parameters are separated, so Equation (9) could be reformed as linear equation

$$\ln\left(\dot{\epsilon}_{cr}(\sigma, t)\right) = \begin{bmatrix} 1 & \ln(\sigma) & \ln(t) \end{bmatrix} \begin{bmatrix} \ln(C_{14}) \\ C_2 \\ C_3 \end{bmatrix} \text{ for } \begin{cases} \sigma_i, i = 1, 2, \dots, 6 \\ t_j, j = 1, 2, \dots, N \end{cases} \quad (10)$$

The creep strain rates shown in Figure 8(b) and the stress of the 6 points in Table 2 are input into Equation (10), by solving this super-determinant, the three creep parameters are then achieved. The final identified creep parameters are presented in Table 3. For these results, it should be noted that the unit of variables in the calculation: stress in MPa, time in second and creep strain rate in micro-strain per second.

Table 3. Identified creep parameters

Creep parameters	C_{14}	C_2	C_3
Identified values	0.43	1.46	-0.59

With all the identified creep parameters, from Equation (2), the equivalent strain rate curves could be plotted, which are compared with the experimental creep strain rates in Figure 9. The experimental ones are plotted by points, while the reconstructed ones by lines. The experimental and calculated curves in same color are of the same point on observed surface. Experimental curves and calculated ones are not superposed, whereas they quite suitable. Even the results should be improved, the above creep parameters could be considered to describe this material's creep properties in the ambient temperature.

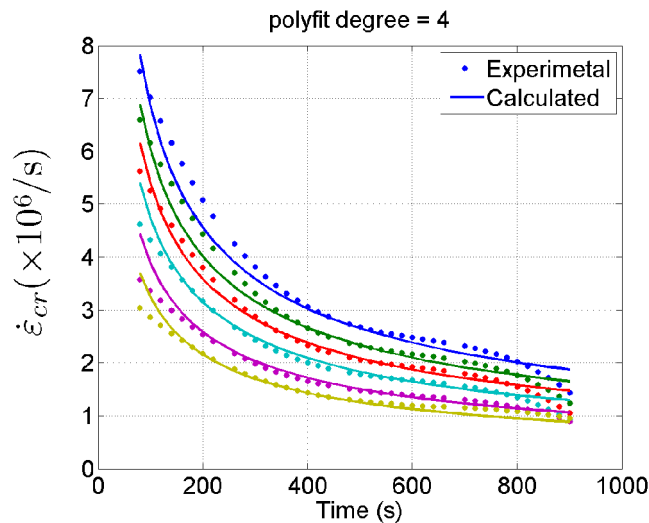


Figure 9. Experimental and calculated creep strain rate curves

4. DISCUSSION

From the above study, the creep behavior of a PBX substitute material is investigated. This material is considered as isotropic material, however the elastic parameters are not quite satisfactory due to multi causes by the 3-points bending test. A classical method, such as tensile/compression test with strain gage maybe give more stable results. For creep test, if the 3-points bending test is applied, the observed zone should be chosen where the deformation is more important. By the research works presented in the literature, the creep time is much longer. If the time interval during image acquisition is longer, the measuring noise would be relatively weaker to the strain fields, therefore its effect would be reduced.

5. CONCLUSION AND PERSPECTIVE

The creep behavior of a PBX substitute material is investigated in this study by full-field analysis. The digital image correlation method could be applied to record the creep deformation. The identified results show that the time-hardening creep model adapts well to this material's creep properties. The measurement should be improved to achieve better identification. In the present study, the reduced parameters of time-hardening model are studied in room temperature. The coming tests would be performed in different temperatures environment, the full four parameters would be investigated.

6. ACKNOWLEDGEMENT

The work is supported by the National Basic Research Program of China through Grant No. 2010CB631005, the National Natural Science Foundation of China (under grants 10625209, 10732080, 90916010), the Project supported by Beijing Natural Sciences Foundation (under grant 3072007), and the authors are also grateful to the opening funds from the State Key Laboratory of Explosion Science and Technology, Beijing Institute of technology.

REFERENCES

1. M. Li, M. Wen, Q. He, et al., "The Compressive Creep Behavior of PBX Based on TATB," *Chinese J. Energ. Mater.* 13 (3), 150–155(2005).
2. P. W. Chen, F. L. Huang, and Y. S. Ding, "Microstructure, deformation and failure of polymer bonded explosives," *Journal of Materials Science*, 42(13), 5272-5280 (2007).
3. Xie HM, Shi H, Chen PW, Liu Z., Dai F., Huang F. "An experimental study on creep deformation of PBX with laser moiré interferometry method," *Key Engineering Materials*, 306-308: 1037-1042 Part 1-2 (2006)
4. Z. W. Liu, H. M. Xie, K. X. Li et al., "Fracture behavior of PBX simulation subject to combined thermal and mechanical loads," *Polymer Testing*, 28(6), 627-635 (2009).
5. B. Pan, K. M. Qian, H. M. Xie et al., "Two-dimensional digital image correlation for in-plane displacement and strain measurement: a review," *Measurement Science & Technology*, 20(6), (2009).
6. B. Pan, and H. Xie, "Full-field strain measurement based on least-square fitting of local displacement for digital image correlation method," *Acta Optica Sinica*, 1980-6 (2007).
7. B. Pan, H. M. Xie, Z. Q. Guo et al., "Full-field strain measurement using a two-dimensional Savitzky-Golay digital differentiator in digital image correlation," *Optical Engineering*, 46(3), (2007).
8. S. Avril, P. Feissel, F. Pierron, P. Villon, "Estimation of the strain field from full-field displacement noisy data" , *European Journal of Computational Mechanics*, Vol 17, N°5-7, pp. 857-868 (2008).
9. M. Grediac, F. Pierron, S. Avril et al., "The virtual fields method for extracting constitutive parameters from full-field measurements: A review," *Strain*, 42(4), 233-253 (2006).
10. S. Avril, F. Pierron, Y. Pannier et al., "Stress reconstruction and constitutive parameter identification in plane-stress elasto-plastic problems using surface measurements of deformation fields," *Experimental Mechanics*, 48(4), 403-419 (2008).
11. S. Avril, M. Grediac, and F. Pierron, "Sensitivity of the virtual fields method to noisy data," *Computational Mechanics*, 34(6), 439-452 (2004).
12. S. Avril and F. Pierron, "Camfit: A Virtual Fields Method Based Software," 2008 SEM XI, (2008).
13. B. Guo, F. Pierron, and R. Rotinat, "Identification of low density polyurethane foam properties by DIC and the virtual fields method," *Proc. SPIE 7375*, 737554-6 (2008).
14. ANSYS Release Documentation, <http://www.ansys.com/>.
15. Tang, W. Li, M. Pang, H.-Y et al., "Creep Model of PBX Based on Modified Time Hardening Theory and its Application," *Chinese Journal Of Explosives And Propellants*, 30(6), 1-4(2007).